Multiwavelength Analysis of a Solar Flare on 2002 April 15

Linhui Sui[1,2], Gordon D. Holman[2], Stephen M. White[3],

and

Jie Zhang[4]

ABSTRACT

We carried out a multiwavelength analysis of the solar limb flare on 2002 April 15. The observations all indicate that the flare occurred in an active region with an asymmetric dipole magnetic configuration. The earlier conclusion that magnetic reconnection is occurring in a large-scale current sheet in this flare is further supported by these observations: (1) Several blob-like sources, seen in RHESSI 12-25 keV X-ray images later in the flare, appeared along a line above the flare loops. These indicate the continued presence of the current sheet and are likely to be magnetic islands in the stretched sheet produced by the tearing-mode instability. (2) A cusp-like structure is seen in NoRH 34 GHz microwave images around the time of the peak flare emission. We quantitatively demonstrate that the X-ray emitting thermal plasma seen with RHESSI had a higher temperature than the microwave emitting plasma seen with NoRH. Since the radio data preferentially see cooler thermal plasma, this result is consistent with the picture in which energy release occurs at progressively greater heights and the hard X-rays see hot new loops while the radio sees older cooling loops. The kinetic energy of the coronal mass ejection (CME) associated with this flare was found to be about one order of magnitude less than both the thermal energy in the hot plasma and the nonthermal energy carried by the accelerated electrons in the flare, as deduced from the RHESSI observations. This contrasts with the higher CME kinetic energies typically deduced for large flares.

Subject headings: Sun: flares—Sun: X-rays

[1]Department of Physics, Catholic University of America, Washington, DC 20064.

[2]Laboratory for Solar and Space Physics, Code 612.1, NASA Goddard Space Flight Center, Greenbelt, MD 20771.

[3]Department of Astronomy, University of Maryland, College Park, MD 20742.

[4]School of Computational Sciences, George Mason University, Fairfax, VA 22030

1. Introduction

It is now widely accepted that magnetic reconnection occurs in the corona to power eruptive solar events such as flares and coronal mass ejections (CMEs) (for an overview see Aschwanden 2004). Magnetic reconnection mechanisms have been studied extensively via theory, but decades of observation have provided only indirect evidence for the reconnection scenario (McKenzie 2002). A number of different magnetic reconnection models have been proposed (Priest & Forbes 2002), but they all predict the existence of one or more current sheets where oppositely directed magnetic field lines converge and reconnect so that magnetic energy is converted into heat and the kinetic energy of energetic particles. Thus, in order to test these magnetic reconnection models, it is crucial to verify the existence of current sheets in flares and the occurrence of magnetic reconnection within them. The difficulty in carrying out this test is the very small thickness predicted for current sheets.

Several flare models (e.g., Forbes & Priest 1995; Shibata et al. 1995; Lin & Forbes 2000), which were developed from the standard 2-D bipolar flare models (Carmichael 1964; Sturrock 1966; Hirayama 1974; Kopp & Pneuman 1976), predict the existence of a large-scale current sheet in flares. On theoretical grounds (e.g., Holman 1985) the current sheet must be very thin – on the order of or much less than a few kilometers – i.e., far smaller than the observational limits of present-day imaging instruments. Nevertheless, these sheets may be directly observable if seen edge on so that a significant emission measure exists along the observational line of sight. Some possible direct observations of large-scale, edge-on current sheets below erupting CMEs have been recently reported (Ciaravella et al. 2002; Ko et al. 2003; Webb et al. 2003; Lin et al. 2005). However, no such observations have been reported in the impulsive phase of solar flares. Some seminal observations, e.g., cusp-shaped soft X-ray flare loops (Tsuneta et al. 1992; Tsuneta 1996), high temperature plasma along the field lines mapping to the tip of the cusp (Moore et al. 1980; Švestka et al. 1987; Tsuneta 1996), and a hard X-ray (HXR) source located above the soft X-ray loops (Masuda et al. 1994, 1995), suggested that the lower tip of the current sheet might be located somewhere at or above the top of the flare loops. However, information on the location of the upper end of the current sheet was missing and it was unclear whether or not a large-scale current sheet exists in flares.

Recently Sui & Holman (2003) found strong evidence for the existence of a large-scale current sheet in an M1.2 flare on 2002 April 15, using observations obtained with the Ramaty High Energy Spectroscopic Imager (RHESSI). The RHESSI images below 20 keV showed a flare loop with a bright looptop and a coronal source above the loop. The coronal source initially appeared to be connected with the loop before the impulsive phase started. Afterwards, the coronal source appeared to detach from the loop and stayed stationary for about

2 minutes before moving outward at $\sim$300 km s^{-1}. Sui & Holman (2003) found that the looptop centroid at high energies was located higher in altitude than the looptop centroid at low energies, while the high-energy part of the coronal source was located lower in altitude than the low-energy part, indicating that the temperature of the underlying loops increased towards higher altitude, and the temperature of the coronal source increased towards lower altitude. These two opposite temperature gradients strongly suggest that the energy release occurred between the flare looptop and the coronal source above, providing strong evidence for the existence of a large-scale current sheet.

Sui & Holman (2003) found another interesting feature in the same flare that also suggests the formation of a current sheet. Decades of observations have indicated an outward expansion of flare loops as the flare progresses. In the standard 2-D flare model (Carmichael 1964; Sturrock 1966; Hirayama 1974; Kopp & Pneuman 1976) and its more modern versions (e.g., Forbes & Priest 1995; Shibata et al. 1995; Lin & Forbes 2000), this outward loop expansion is interpreted as an apparent motion, reflecting a shift of emission to higher, newly reconnected field lines. However, in the 2002 April 15 flare, Sui & Holman found that before the X-ray loop started to move outward, the apparent source altitude decreased at $\sim$9 km s^{-1} in the early impulsive phase of the flare. This downward motion lasted for $\sim$2 min. It is not predicted by the standard 2-D reconnection models. Sui & Holman interpreted this decrease in altitude to be due to the change of the magnetic field configuration as the X-point collapsed into a current sheet. Another possibility is that the loop shrinkage is the observation of the relaxation of newly reconnected field lines before the outward buildup of the newly reconnected loops becomes dominant (Sui, Holman & Dennis 2004; Lin 2004). Recently, Veronig et al. (2005) showed that a collapsing magnetic trap model (Karlický & Kosugi 2004) could explain this downward motion.

Two other flares, one on 2002 April 14-15 and the other on April 16, occurred in the same active region as the 2002 April 15 flare. They share some common features with the flare on April 15 (Sui, Holman & Dennis 2004): (1)A coronal source up to $\sim$ 30″ above the flare loop appeared before the impulsive phase started. For the April 16 flare, the coronal source above the flare loop had an energy gradient similar to that of April 15 (Sui 2005), i.e., the high-energy part of the coronal source was located lower in altitude than the low-energy part. (2) Before the flare loop moved upward, the flare looptop centroid moved downward for 2–4 minutes during the early impulsive phase of the flare, falling by 13–30% of its initial height with a speed in the range of 8–23 km s^{-1}. All these features were considered to be related to the formation and/or the development of the current sheet (Sui, Holman & Dennis 2004).

In this paper, we further study multiwavelength observations of the 2002 April 15 event

to determine whether they are consistent with the formation of the large-scale current sheet previously inferred from the RHESSI data alone. We also compare the energies of the flare heated plasma and accelerated electrons with the kinetic energy of the associated CME. We make use of observations from the following instruments: RHESSI, the Nobeyama Radioheliograph (NoRH), the Transition Region and Corona Explore (TRACE), the Michelson Doppler Imager (MDI) and Large Angle and Spectrometric Coronagraph (LASCO) on board the Solar and Heliospheric Observatory (SOHO).

2. Observations and Data Analysis

RHESSI and TRACE observations of the flare, and LASCO observation of the CME, are described in § 2.1. The NoRH microwave observations are described and then compared with the RHESSI observations in § 2.2. The flare and CME energetics are discussed in § 3. We discuss and summarize our results in § 4.

2.1. RHESSI, TRACE and LASCO Observations

2.1.1. RHESSI images

RHESSI X-ray light curves in two energy bands (6–12 and 25–50 keV) are shown in the top panel of Figure 1. The 6–12 keV flux started to rise at ∼23:02 UT. The HXR flux (>25 keV), after a minor increase starting at 23:07 UT, rose abruptly at 23:09:40 UT, indicating the start of the impulsive phase. The impulsive phase lasted for ∼8 min until 23:17:30 UT, when the 25-50 keV count rate returned to the pre-flare level. RHESSI stopped observations after 23:20 UT because of its entry into the South Atlantic Anomaly (SAA). The gradual flux decrease in the 25-50 keV band before the start of the flare was due to the high particle background, while the gradual flux increase in the same energy band after the impulsive phase was caused by the entry into the SAA.

A sequence of RHESSI 10–20 keV images is shown in Figure 2. The images are dominated by the emission from a flare loop with its northern leg longer than the southern leg, indicating an asymmetric loop structure. The coronal source appeared above the loop after first being connected with the loop in the rise phase of the flare (first two panels in Fig. 2). After staying stationary for about 2 min, the source moved upward with a speed of ∼300 km s^{-1} and later disappeared from the RHESSI images.

A CME was identified to be associated with this flare. As indicated by SOHO/LASCO

C2 and C3 difference images (Fig. 3), a large coronal loop visible up to $\sim$17 $R_\odot$ propagated outward at an average speed of $\sim$300 ($\pm$100) km s^{-1}. The height-time plot for the outward moving coronal source seen in the RHESSI images and the CME seen in the LASCO C2/C3 images is shown in Figure 4. Extrapolating forward in time from the RHESSI images with this velocity puts the outward moving coronal source seen in RHESSI at the leading edge of the coronal loop seen in the LASCO C2 image at 02:26 UT on April 16 (Fig. 3, left panel). This suggests that the outward moving coronal source seen with RHESSI has a strong connection with the CME.

RHESSI images in different energy bands at the flare HXR peak (23:11–23:12 UT) are shown in Figure 5. The RHESSI images below 20 keV show a bright looptop, while the images at higher energies show a looptop source plus two additional sources that we interpret as footpoints of the same loop. The centroid of the looptop source at high energies is located higher than at low energies (Sui & Holman 2003). The footpoints and the HXR looptop source can be seen during most of the impulsive phase (from 23:09:40 to 23:13 UT). The HXR looptop source is brighter in this energy than either footpoint except at the major peak, while most of the HXR looptop sources previously reported were weaker relative to the footpoints (e.g. Masuda et al. 1994, 1995; Petrosian, Donaghy, & McTiernan 2002; Sui et al. 2002). Veronig & Brown (2004) attributed this bright HXR looptop source to thick-target bremsstrahlung from nonthermal electrons in the corona. An extra footpoint mentioned by Sui & Holman (2003) was carefully checked (e.g., using 'CLEAN boxes' when reconstructing the CLEAN image[1]) and appears not to be a real footpoint. The simpler two-footpoint loop configuration is also consistent with the TRACE images shown below.

The two footpoints were not of equal brightness. The southern footpoint (SF) was brighter than the northern footpoint (NF) (See Fig. 5). This asymmetry is probably caused by the asymmetry in the photospheric magnetic field strength (?Sakao et al. 1996). The electrons precipitating into the footpoint with the stronger magnetic flux suffer more severe magnetic mirroring, therefore emitting weaker HXR emission at that footpoint. This interpretation is consistent with the longitudinal magnetogram obtained with the SOHO/MDI shown in Figure 6. The maximum line of sight magnetic field strengths near the northern and southern footpoints are -380 and +280 Gauss, respectively. However, Siarkowski & Falewicz (2004) reported quasi-periodic changes in the asymmetry of two footpoint fluxes in an X-class flare observed with the Yohkoh Hard X-ray Telescope (HXT). They suggested that the footpoint asymmetry in their case might be due to asymmetric injection of electrons from the top of the flaring loop.

---

[1]The instructions for making CLEAN images with 'CLEAN boxes' can be found at http://sprg.ssl.berkeley.edu/~krucker/hessi/clean_tut.html

2.1.2. TRACE Observations

The TRACE 1600 Å channel is sensitive to plasma in the temperature range between 4 and 10×10^3 K (Handy et al. 1999). Therefore, emissions in this channel come mainly from the chromosphere where the footpoints and ribbons are located. The TRACE 195 Å channel is sensitive to higher temperature (5.0–20×10^5 K, and 1.1–2.6×10^7 K) plasma, but it was not used during this flare.

In the rise phase of the flare (before 23:09:40 UT), TRACE 1600 Å images show two ribbons (Fig. 7, left panel). The northern ribbon is about $30''$ long, with the northeast end brighter than the rest of the ribbon; the southern ribbon is about $20''$ long, but brighter than the northern one. The overlaid RHESSI 10–20 keV image suggests that the X-ray loop connects the two ribbons.

When the impulsive phase started, a small, bright kernel in 1600 Å emission suddenly appeared in the middle of the northern ribbon (Fig. 7, right panel). It is co-spatial with the northern footpoint seen in the RHESSI images. The large kernel that was present in the southern ribbon before the impulsive phase also brightened at the same time. This large kernel is almost co-spatial (within $\sim 5''$) with the southern footpoint seen in RHESSI images. The intensity of the kernels in 1600 Å increased at the same times that the RHESSI 25–50 keV flux increased. In the decay phase, those distinct kernels along the two ribbons gradually disappeared, and the ribbons became more uniformly bright but with the southern ribbon still brighter than the northern one.

In the right panel of Figure 7, there is an additional, weaker 1600 Å source to the west of and connected to the southern ribbon. This source appeared soon after the impulsive phase started. Its intensity and location did not change for more than 20 min. This evolution indicates that this source is chromospheric and not directly associated with the X-ray looptop source and the coronal source above the looptop, because both of these X-ray sources existed before the start of the impulsive phase and involved differently.

2.1.3. Magnetic Islands in the Current Sheet

As introduced in §1, Sui & Holman (2003) proposed that a large-scale current sheet was formed between the coronal source above the flare loop and the HXR looptop source. The coronal source moved outward at a speed of ~ 300 km s^{-1}, while the loop moved at only ~ 10 km s^{-1} (Sui & Holman 2003; Sui, Holman & Dennis 2004). Thus, the current sheet must have continuously elongated. This elongation of the current sheet is incorporated in various flare models (see a review by Priest & Forbes 2002).

Furth, Killeen, & Rosenbluth (1963) showed that a current sheet can be unstable to the tearing-mode instability. They predicted that a stretched current sheet becomes unstable to the tearing mode after its length exceeds about 2π times its width. The tearing mode will change the magnetic topology along the current sheet such that blob-like magnetic island structures appear. This could explain the bursty and intermittent pulses (on time scales of seconds or subseconds) of particle acceleration seen in HXRs and radio wavelengths (Aschwanden 2002). Signatures of the tearing mode have been seen in Tokomaks, and we speculate that, for the first time, we have detected them in the RHESSI images of this flare.

With a speed of 300 km s^{-1}, the outward moving coronal source above the loop must have exited the RHESSI image field of view at around 23:13 UT (see Fig. 2). However, the RHESSI 10–20 keV images between 23:13 UT and 23:18 UT show several faint blob-like sources along the trajectory of the initial coronal source above the flare loop. Two such images are plotted in Figure 8 where the trajectory of the original coronal sources is shown as a dotted line in each image. Although the location of these sources changed from time to time, they were always located along this trajectory within $\sim$3 arcsec. Therefore, these blob-like sources are evidence for the growth of an instability within the current sheet. The most likely instability is the tearing-mode instability because, as stated above, it is expected to occur as the sheet lengthens and it can produce distinct magnetic blobs with enhanced local heating of the plasma.

It is possible that these blobs could be artifacts of the RHESSI image processing. But the appearance of these blobs in the expected location, at different times, in different energy bands constructed with different imaging algorithms all argue against this possibility. The ongoing efforts by the RHESSI team to improve the dynamic range of RHESSI images should eventually allow us to further study the nature of these sources.

2.2. NoRH Observations

Because gyrosynchrotron microwave emission and HXR bremsstrahlung are both produced by highly energetic electrons, but with different emission mechanisms, the observations in these two wavelength regimes offer us information on different aspects of conditions in the solar atmosphere where flares occur (White et al. 2003). Bremsstrahlung is produced by collisions between accelerated electrons and ambient plasma; thus the intensity depend on their densities. Gyrosynchrotron microwave radiation depends on the magnetic field intensity and its direction. The gyrosynchrotron production mechanism is extremely efficient, allowing us to detect electrons at energies of hundreds of keV, even when their numbers are very low. Microwave emission can also be produced by thermal electrons through bremsstrahlung in

sufficiently dense thermal plasma, similar to the production of soft X-rays.

This flare was observed by NoRH at 17 and 34 GHz. We made maps with 1 s time resolution and spatial resolutions of 12″ at 17 GHz and 8″ at 34 GHz. The dynamic range of NoRH images can be $>\sim$200:1, i.e. much better than $\sim$20:1 currently achieved with RHESSI.

2.2.1. NoRH Microwave Observations

The time profiles of the microwave flux at 17 and 34 GHz, shown in the lower panel of Figure 1, were obtained from images with constant background subtracted. Evidently, the time profiles at the two frequencies are different in the rise and impulsive phases of the flare. The 17 GHz flux increased slowly as early as 23:02 UT, when the RHESSI 6-12 keV flux started to increase. It is striking that from 23:07 to 23:09:40 UT, just before the impulsive rise, even the very small flux increase in the RHESSI 25–50 keV band corresponds to a simultaneous flux increase at 17 GHz. The spikes at 17 GHz during the impulsive phase correlate very well with the spikes in the RHESSI 25–50 keV band, suggesting that the 17 GHz emission was gyrosynchrotron radiation from predominantly nonthermal electrons. During the decay phase (after 23:16 UT), the X-ray flux below 25 keV was decreasing, while the 17 GHz flux maintained a level 5 times the background and increased slowly until 23:23 UT. This difference in time profiles suggests that the 17 GHz flux in the decay phase is predominantly bremsstrahlung from thermal plasma, but originating in a plasma at a temperature different from that of the hard X–ray–emitting plasma (we study this difference in more detail below).

Unlike the 17 GHz flux, the 34 GHz flux did not significantly increase until the impulsive phase started at 23:09:40 UT. During the impulsive phase, the 34 GHz fluxes increased gradually and steadily, except for a short spike around 23:11:30 UT, which corresponded to the major peak in both the 17 GHz flux and the RHESSI 25–50 keV HXR flux. The fluxes at 17 and 34 GHz after 23:16 UT were about equal, indicating a flat (thermal) spectrum. Both the 17 and 34 GHz fluxes had a secondary peak around 23:23 UT. Notice that the general 34 GHz time profile is similar to that of the GOES 1–8 Å Soft X-ray (SXR) flux (except at the major HXR peak), further suggesting that the 34 GHz flux was predominately thermal during most of the flare.

The NoRH microwave maps at 17 and 34 GHz shown in Figure 9 are morphologically different from one another, except in panel G. The images at the two frequencies reveal the evolution of different microwave radiation mechanisms throughout the flare. Starting

at 23:00 UT, the 17 GHz images suggest some emission from both the active region where the flare occurred and coronal sources above it. They look very different from the later images when the flare was fully developed. After 23:05 UT, the 17 GHz images show two ends of a flare loop, with the northern end much brighter than the southern end (panel A in Fig. 9). As pointed out in § 2.1, the longitudial magnetic field near the northern footpoint was stronger. The rise in emission at 17 GHz prior to the impulsive phase that is not seen at 34 GHz can be attributed to electrons accelerated to energies high enough to produce relatively low-harmonic gyrosychrotron radiation but not high enough to produce significant gyrosynchrotron emission at 34 GHz. When the impulsive phase started at 23:09:40 UT, the 17 GHz images (panels B, C, & D) were still dominated by footpoint emissions, with the northern footpoint still much brighter than the southern one. The 17 GHz images between 23:16 and 23:26 UT show the two footpoints with comparable brightness and some emission from the entire loop (panel E), suggesting a different radiation mechanism: thermal free-free emission. This interpretation is in agreement with the gradual time profile after 23:16 UT, and with the similarity of the time profile to the GOES SXR behavior. All the images after 23:26 UT show only the flare loop, with the southern half of the loop brighter than the northern half (panel G). This is presumably because the emission measure of the plasma observed in microwaves in the southern leg is larger, in agreement with RHESSI and TRACE 1600 Å images showing a larger southern footpoint relative to the northern one.

The 34 GHz images do not show any identifiable source until the start of the impulsive phase at 23:09:40 UT (panel A). This is consistent with the flat time profile due to the background emission. Between 23:09:40 and 23:11:10 UT (panels B & C), all the 34 GHz images show the flare loop. The two footpoints of the flare loop were brighter than the rest of the loop, but had comparable brightness. These images suggest thermal free-free emission, in agreement with the gradual flux increase in the time profile during that period. The two bright loop footpoints, which are similar to the 34 GHz images between 23:16 and 23:26 UT when free-free emission dominated, indicate that the density of the plasma contributing to the microwave emission is higher at the footpoints. The images between 23:11:20 and 23:11:50 UT (panel D), when the 34 GHz time profile had a spike, were dominated by the emission near the two ends of the loop, but with the northern end brighter than the southern one, suggesting the presence of electrons with sufficient energy (above 100 keV) to produce nonthermal gyrosynchrotron radiation at both 17 and 34 GHz. All the images after 23:11:50 UT show the flare loop (Panels E & F), with the southern half of the loop being brighter than the northern half, as is also seen in the 17 GHz images after 23:26 UT.

2.2.2. Cusp Structure in the Microwave Images

Besides the flare loop and footpoints, the NoRH images at both 17 and 34 GHz all show a cusp-like structure above the loop during the impulsive phase. The cusp can be seen in the 17 GHz images around the HXR peak of the flare (Fig. 10, lighter contours) and in the 34 GHz image at 23:11:20 UT (as indicated by an arrow in panel D of Fig. 9).

Further analysis indicates that the cusp-like structure at 17 GHz during the HXR peak might be free-free emission from the coronal source above the active region, which existed before the flare started. As we mentioned earlier, in the early rise phase between 23:00–23:05 UT, the 17 GHz images showed some emissions from the active region and from the coronal sources above. To check whether or not the coronal source in the pre-flare phase contributes to the emission seen in the vicinity of the cusp during the flare, we subtract the average of the 17 GHz images during the period 23:00–23:05 UT (Fig. 10, panel a) from the images near the flare peak (Fig. 10, light contours in panels b to f), and found that the cusp was not prominent in the subtracted images (Fig. 10, dark contours in panels b to f). This suggests that much of the apparent emission from the cusp location at 17 GHz is active region free-free emission that was present along this line of sight prior to the flare.

In contrast, we subtracted the average of the 34 GHz images during the period 23:00–23:05 UT from the 34 GHz image at the 23:11:20 UT, but in this case the cusp remains clearly visible in the subtracted images. This is because of the fact that the 34 GHz images do not show any source identifiable with the cusp during the rise phase. A 34 GHz image at 23:08:30 UT showing background emissions is plotted in Figure 9 (panel A). The background-subtracted images are almost exactly the same as those original images. This indicates that the cusp in the 34 GHz images was associated with the flare, not pre-existing coronal features.

2.2.3. Comparison of Microwave Images With X-ray Images

The two footpoints seen with NoRH and RHESSI have the opposite flux asymmetries. The southern footpoint is stronger of the two in the RHESSI images, but it is the weaker footpoint in the NoRH images. This suggests that the magnetic field near the northern footpoint is stronger than the field near the southern footpoint, in agreement with the MDI magnetogram.

NoRH 17 GHz and RHESSI 20–50 keV images both show the emissions from the non-thermal electrons during the impulsive phase of the flare. But the 17 GHz images are more sensitive for detecting these energetic electrons. This was particularly important in detecting the weak electron fluxes before the impulsive phase started. As indicated in the RHESSI

light curve (Fig. 1, upper panel), there was some weak HXR flux in the 25–50 keV band starting at 23:07:00 UT over ∼2 min before the start of the impulsive phase. But the flux was too low for the 25–50 keV images to show any identifiable source. In contrast, the 17 GHz images as early as 23:05 UT, almost 5 min before the impulsive phase of the flare started, show emission from the two footpoints of the loop, with the northern one much brighter than the southern one.

The brightness peak of the RHESSI 10–20 keV images and most of the 34 GHz images (when thermal emission dominated, i.e., before 23:11:20 UT and after 23:11:30 UT) are located in different places in the loop. The peak of the RHESSI 10–20 keV images is always located in the looptop region (Fig. 11), while the peak in the 34 GHz images (Fig. 9, panels B, C, E, and G) is located either near the two footpoints or in the southern half of the loop. In the standard flare models (Carmichael 1964; Sturrock 1966; Hirayama 1974; Kopp & Pneuman 1976), the magnetic reconnection occurs above the flare loops, and consequently the looptop region is hotter than the rest of the loop. Thus, the plasma producing thermal emission observed in microwaves is most likely cooler than the plasma producing the X-rays seen with RHESSI.

The flare loop in the X-ray images was located higher than that in the microwave images during the decay phase after 23:16 UT. In the impulsive phase (panels B, C and D of Fig. 11), the loop in the 10-20 keV images (dark contours) seems to be co-spatial with that in 34 GHz (light contours). However, in the decay phase (panels E and F), the loops in the RHESSI images are located higher than the loops in the NoRH images. This is particularly evident in panel F, where the RHESSI loop was ∼10 arcsec higher. This difference in loop location again is consistent with the hypothesis that RHESSI is more sensitive to the higher-temperature plasma than NoRH.

The apparent upward expansion of flare loops seen in the RHESSI images (Sui & Holman 2003; Sui, Holman & Dennis 2004) is also evident in microwaves, while downward motion is not seen. As indicated in Fig. 9, the flare loops in 17 and 34 GHz moved upward as the flare progressed. A rough estimate of the speed is ∼4 km s^{-1}, which is slower than the upward motion speed (∼8–21 km s^{-1}) seen in the RHESSI images (Sui & Holman 2003; Sui, Holman & Dennis 2004). This slower speed explains why the loops in microwaves are located lower in altitude than those seen in X-rays during the decay phase of the flare. We also checked for downward motion using the 34 GHz images between 23:09:40 and 23:11:30 UT, when the downward motion was seen in the RHESSI images, but again, no obvious downward motion was detected.

In the next section, we quantitatively demonstrate that the plasmas seen by GOES and RHESSI could not produce enough microwave emission to account for the microwave fluxes

observed with NoRH. This can also explain why the coronal source above the flare loops seen in the RHESSI 10–20 keV images (Fig. 2) did not appear in any of the NoRH images.

2.3.   Comparison of Predicted and Observed Free-Free Microwave Fluxes

Based on the NoRH time profile and images, we have concluded that thermal bremsstrahlung dominated the emission at 34 GHz except at the major peak around 23:11:30 UT, when the emission was gyrosychrotron. The differences between the RHESSI 10–20 keV and the 34 GHz images, as discussed above, further indicate that the plasma seen with RHESSI is hotter than that seen by NoRH. To quantitatively test this hypothesis, we calculated the predicted microwave flux emitted by the plasma observed with RHESSI and GOES, and compare it with the NoRH measured flux at 34 GHz.

Before calculating the flux of free-free emission, we first check whether the emission at 17 and 34 GHz was optically thin or thick. The optical depth (τ) of hot coronal plasma at frequency ν (GHz) is calculated with the formula (Lang 1999):

$$\tau(\nu) = 98 \cdot \frac{EM(17.7 + log\frac{T^{1.5}}{\nu})}{T^{1.5}\nu^2 A} \tag{1}$$

where T is the plasma temperature (MK), EM is the emission measure (10^{49} cm^{-3}), and A is the emitting source area (10^{18} cm^2). Recently, Sui, Holman & Dennis (2005) have obtained T and EM of the thermal plasma for this flare from GOES and RHESSI observations (see Fig. 6 of Sui, Holman & Dennis 2005). The GOES T and EM were obtained using the code developed by White, Thomas, & Schwartz (2005), based on the Chianti atomic model (Young et al. 1998). The RHESSI T and EM were obtained by fitting spatially integrated RHESSI spectra. During the decay phase of the flare, typical EM and T obtained with RHESSI are $\sim 10^{48}$ cm^{-3} and 20 MK, respectively. The source area estimated from the NoRH images is $\sim 7 \times 10^{18}$ cm^2. According to equation (1), the optical depths at 17 and 34 GHz are 10^{-3} and 2×10^{-4}, respectively, i.e., much less than 1, indicating that the emission at both 17 and 34 GHz is optically thin.

We compute the expected 34 GHz flux using the following formula for optically thin free-free emission (Lang 1999):

$$F(\nu) = 1.3 \cdot \frac{EM}{\sqrt{T}}(17.7 + log\frac{T^{1.5}}{\nu}) \tag{2}$$

where $F(\nu)$ is the microwave flux (10^{-22} watt m^{-2} Hz^{-1}, or sfu) at frequency ν (GHz). Using the T and EM obtained with GOES and RHESSI, the predicted 34 GHz fluxes from the

plasma observed with GOES and RHESSI are plotted in Figure 12. The NoRH observed 34 GHz flux after 23:09:30 UT is also plotted (solid line). Since the 34 GHz flux did not significantly increase until 23:09:30 UT, the average flux during 23:00–23:05 UT, believed to be preflare background flux) was subtracted from the observed 34 GHz flux. It is evident that the predicted fluxes are less than the NoRH observed flux by a factor of 4 to 5. The predicted fluxes from GOES and RHESSI are comparable during most of the flare, although the flux predicted by RHESSI peaks ∼4 min earlier, consistent with RHESSI seeing hotter plasma. Based on equation (2), in order to account for the observed microwave emission, we need to decrease T and/or increase EM. Thus, we conclude that the radio emission seen after the impulsive phase is thermal emission from a plasma with a temperature lower than that of the plasma producing the X–rays. This agrees with the finding of Chertok et al. (1995) that the main contribution to the microwave bursts (if they are due to optically-thin thermal bremsstrahlung) comes from evaporating, denser 'warm' plasma with a temperature less than that of X-ray emitting plasma.

Since the microwave flux of free-free emission is not sensitive to the frequency ν, the discussion above also applies to 17 GHz. This means that during the decay phase of the flare, the NoRH-observed 17 GHz flux must also be produced by cooler plasma.

3. Flare and CME Energetics

Solar flares and CMEs are believed to be two different manifestations of the same energy release process (i.e., magnetic reconnection) in the solar corona. Therefore, a reliable estimate of energy partition between the flare and CME provides constraints on the energy release process (Emslie et al. 2004).

The peak thermal energy and the total nonthermal electron energy of this flare have recently been calculated by Sui, Holman & Dennis (2005). A low-energy cutoff of 24 keV to the distribution of accelerated electrons was determined with an uncertainty of ± 2 keV from a combination of spectra, images, and lightcurves derived from RHESSI data alone. As a result, the total energy in the nonthermal electrons was estimated to be 1.6 (± 1) $\times 10^{30}$ ergs, compared with the peak thermal energy of $\sim 6 \times 10^{29}$ ergs estimated from both GOES and RHESSI data. The uncertainty for the nonthermal energy was based on the low-energy cutoff uncertainty of ± 2 keV.

Using the method proposed by Vourlidas et al. (2000), the mass of the ejected large coronal loop in Figure 3 is estimated to be 5 (± 2.5) $\times 10^{13}$ grams. The projected velocity of the CME is 300 (± 100) km s^{-1}. Therefore, the kinetic energy of the CME is $\sim 2(^{+4}_{-1.7})$

$\times 10^{28}$ ergs. The kinetic energy of the CME is about one order of magnitude less than both the thermal energy of the plasma and the nonthermal energy in the accelerated electrons. This result is opposite to the results of Emslie et al. (2004). For the two big events they analyzed (X4.8 flare on 2003 July 23 & X1.5 flare on 2002 April 21), both the thermal and nonthermal flare energies, estimated from RHESSI observations, were half to a whole order of magnitude smaller than the CME energy. However, the uncertainty of these energies is still large Emslie et al. (2005). These limited studies may suggest that flare energies are poorly correlated with associated CMEs. A statistical study of 249 CMEs observed with the Solar Maximum Mission Coronagraph (Hundhausen 1999) indicated that the kinetic energy of CMEs correlated poorly with the SXR peak intensities of the associated flares. Hundhausen (1999) pointed out that, given the intensity of a flare, the kinetic energy of its associated CME can still be spread over a range of at least three orders of magnitude.

4.   Summary and Discussions

Sui & Holman (2003) presented strong evidence for the existence of a large-scale current sheet in the M1.2 flare on 2002 April 15. In order to further test this conclusion, we have analyzed this event with additional observations from RHESSI and other instruments. Several aspects of these observations have been found to be consistent with the predictions of the 2-D standard flare models (e.g., Forbes & Priest 1995; Shibata et al. 1995; Lin & Forbes 2000).

The observations indicate that a dipole magnetic configuration is involved in the flare. A nonsymmetrical flare loop, consistently revealed by the RHESSI, TRACE, and NoRH images, connects the opposite magnetic polarities. The two footpoints in the RHESSI and NoRH images coalign well with the bright kernels in the two ribbons seen in the TRACE 1600 Å images. The RHESSI images indicate that the southern footpoint of the flare loop is brighter than the northern one. However, the NoRH microwave images show the opposite. With the consideration of magnetic mirroring (Kundu et al. 1995), this apparent contradiction can be reconciled if the magnetic field near the northern footpoint was stronger than the southern footpoint. The MDI magnetogram is indeed consistent with this asymmetric magnetic configuration.

Further analysis of the RHESSI images suggest that tearing-mode-like islands are seen, consistent with the presence of the large-scale current sheet claimed by Sui & Holman (2003) for this event. Furth, Killeen, & Rosenbluth (1963) predicted that when a current sheet is stretched it would become unstable to the tearing-mode instability, resulting in blob-like magnetic island structures along the current sheet. During the decay phase of the flare, the

RHESSI 12–25 keV images showed several faint, blob-like sources along the trajectory of the initial coronal source. Although the location of these sources changed from time to time, they were always located along this trajectory. Most importantly, the presence of these blobs indicates the continuing existence of the current sheet.

The true size of magnetic islands should be much smaller than the size of the blob-like sources (i.e., $\sim$10–15 arcsec) seen in the RHESSI images. Because the current sheet is very thin ($<$1 arcsec), the size of the magnetic islands should be less than, or at most equal to, the thickness of the current sheet, even considering the possibility that some of magnetic islands may collapse into each other due to the nonlinear tearing-mode instability (Carreras et al. 1980). Two possible reasons why we see these relatively large sources are: (1) The blobs were not resolved due to the current RHESSI imaging limitation. When one bright, large source (e.g., the X-ray looptop) and one faint, smaller source are in the same RHESSI image, it is impossible to resolve the smaller source using any of the existing RHESSI imaging algorithms, because imaging with finer grids (say, grid 1 with 2.3 arcsec resolution) will over-resolve the larger, brighter source, and thus cause the whole image to break up. (2) The current sheet was not observed exactly edge-on. The size of the islands would be larger if they were significantly extended along the width of the current sheet. Ko et al. (2003) and Lin et al. (2005) reported LASCO C2/C3 observations of multiple blob-like sources moving in a long, thin streamer-like feature in two flare-associated CMEs. They interpreted those blobs as outflow plasma from a continuously reconnecting current sheet about a few hours after the impulsive phase of the associated flares.

The 34 GHz microwave observations show a cusp-like feature above the flare loop. Such a cusp-like structure above the flare loop, previously observed with Yohkoh Soft X-ray Telescope (SXT) (e.g., Tsuneta et al. 1992; Tsuneta 1996), is believed to indicate a kink in the reconnected magnetic field lines, suggesting the existence of the current sheet. One of the 34 GHz NoRH images near its peak shows a cusp-like feature above the loop. However, neither the coronal source above the loops in the impulsive phase found by Sui & Holman (2003) nor the blob-like sources discussed here appeared in any of the microwave images. The absence of these sources in the microwave images could be due to the fact that the thermal emission detected with RHESSI is produced by plasma with higher temperatures than that producing the microwaves. This also explains the difference in appearance of the thermal sources in the RHESSI and NoRH images, such as the greater height of the SXR loops in the decay phase.

We do not find the interpretation of the coronal HXR source as thick target bremsstrahlung by Veronig & Brown (2004) to be in conflict with the radio observations. Veronig & Brown (2004) estimated the peak plasma density inside of the loop to be around 5×10^{10} cm^{-3}. The

plasma frequency associated with this density is around 2 GHz. This is well below the NoRH observation frequencies of 17 and 34 GHz. However, if reconnection continuously forms new loops as expected in the standard models, the thick-target interpretation does require the reconnecting loops to be dense even before reconnection occurs, because chromospheric e-vaporation typically needs tens of seconds to minutes to fill a loop (Antonucci et al. 1990, and references therein).

The apparent upward expansion of the flare loops was seen in microwaves, in agreement with the RHESSI results. However, the expansion speed in microwaves ($\sim$4 km s^{-1}) was much slower than the speed in X-rays ($\sim$8–21 km s^{-1}). This difference in speed is consistent with the argument that thermal microwave emission is radiated from the cooler loops. The loop shrinkage found in the RHESSI images was not detected by NoRH. This could be due to the following two reasons. First, unlike the RHESSI images, the microwave images do not have a bright looptop. Instead, the two legs or footpoints are brighter than the rest of the loop. Thus, it is very difficult to determine the loop altitude as precisely as we did with the loops in the RHESSI images. The X-ray loop shrinkage was only $\sim$2–3 arcsec for this event (Sui & Holman 2003; Sui, Holman & Dennis 2004). Second, the microwave images show the emission from loops filled with the cooler plasma, which reconnected much earlier than the hot loops seen in X-rays. Therefore, the shrinkage caused by the formation or development of the current sheet would not affect the cooler, lower microwave loops as much as the hotter, higher X-ray loops.

We have also compared the kinetic energy of the CME associated with this flare with the energy contained in the thermal plasma observed in X-rays and in accelerated electrons. The energy contained in both the hot plasma and the accelerated electrons was found to be about one order of magnitude larger than the kinetic energy of the CME. For the two events analyzed by (Emslie et al. 2004), the CME kinetic energies were found to be almost one order of magnitude larger than both the flare thermal and nonthermal energies. The analysis of this limited number of cases suggests that the flare energy and the kinetic energy of the associated CME may not correlate with each other. However, a recent statistical study by Burkepile et al. (2004) showed that there might be a correlation between 'limb' CMEs and soft X-ray peak flux from associated flares. Nevertheless, the correlation is rather poor. For a particular flare class, CME kinetic energy may vary by orders of magnitude.

It is worthwhile to emphasize that the thermal energy of the flare was taken as the peak thermal energy during the flare. The energy losses due to radiative and conductive cooling were not included in the calculation. Therefore, the total flare thermal energy could be underestimated by an order of magnitude Emslie et al. (2005). With energy losses included, the energy budget results of Emslie et al. (2004) may changed significantly. However, for

the flare we analyzed here, the thermal energy of the flare will be even larger than we have presented and, therefore, still larger than the kinetic energy of the CME.

To conclude, we want to point out that although the modern versions of the 2-D standard flare model can explain several aspects of the observation in this flare, there are other observations which are beyond the model predictions, such as the loop shrinkage and the above-the-loop coronal source staying stationary for a few minutes before moving outward (Sui & Holman 2003; Sui, Holman & Dennis 2004). Moreover, the detectability of current sheets and magnetic islands has not been studied in the framework of the 2-D models either. We hope the observations presented here will inspire some further studies in these regards.

REFERENCES

Antonucci, E., Dodero, M. A., Martin, R. 1990, Sol. Phys., 73, 147

Aschwanden, M. J., Hudson, H. S., Kosugi, T., & Schwartz, R. A. 1996, ApJ, 464, 985

Aschwanden, M. J. 2002, Particle Acceleration and Kinematics in Solar Flares, Kluwer Academic Publishers

Aschwanden, M. J. 2004, Physics Of The Solar Corona, Praxis Publishing Ltd.

Bruzek, A. 1964, ApJ, 140, 746

Burkepile, J. T., Hundhausen, A. J., Stanger, A. L., St. Cyr, O. C., Seiden, J. A. 2004, JGR, 109, A03103

Carmichael, H. 1964, In The Physics of Solar Flares, ed. W. N. Hess (NASA SP-50, Washington, DC:NASA), 451

Carreras, B. A., Hicks, H. R., Homes, J. A., and Waddell, B. V. 1980, Phys. Fluids, 23, 1811

Chertok, I. M., Fomichev, V. V., Gorgutsa, R. V., Hildebrandt, J., Kruger, A., Magun, A., Zaitsev, V. V., 1995, 160, 181

Ciaravella, A., Raymond, J. C., Li, J., Reiser, P., Gardner, L. D., Ko, Y.-K., & Fineschi, S. 2002, ApJ, 575, 1116

Emslie, A. G., Kucharek, H., Dennis, B. R., Gopalswamy, N.; Holman, G. D., Share, G. H., Vourlidas, A., et al. 2004, J. Geophys. Res., 109, A10104

Emslie, A. G., Dennis, B. R., Holman, G. D., Hudson, H. S., 2005, J. Geophys. Res., submitted

Forbes, T. G., & Priest, E. R. 1995, ApJ, 446, 377

Furth, H.P., Killeen, J., & Rosenbluth, M.N. 1963 Finite-resistivity instabilities of a sheet pinch, Phys. Fluids, 6, 459

Handy et al. 1999, Sol. Phys., 187, 229

Hirayama, T. 1974, Sol. Phys., 34, 323

Holman, G. D. 1985, 293, 584

Hundhausen A. J., 1999, Coronal Mass Ejections, AGU Geophysical Monograph 99, Eds: Nancy Crooker, Jo Ann Joselyn, Joan Feynman, P1-7

Hurford, G.J., et al. 2002, Sol. Phys., 210, 61

Karlický, M, & Kosugi, T. 2004, A&A, 419, 1159

Kopp, R.A., & Pneuman, G.W. 1976, Sol. Phys., 50, 85

Ko, Y.-K., Raymond, J.C, Lin, J., Lawrence G., Li, J., Fludra, A. 2003, ApJ, 594, 1068

Kundu, M. R., Nitta, N., White, S. M., Shibasaki, K., Enome, S., Sakao, T., Kosugi, T., & Sakurai, T., 1995, ApJ, 454, 522

Krucker, S., & Lin, R. P. 2002, Sol. Phys., 210, 229

Lang, K. R. 1999, Astrophysical Formulae, Springer

Lin, R.P., et al. 2002, Sol. Phys., 210, 3

Lin, R.P., et al. 2003, ApJ, 595, L69

Lin, J., & Forbes, T.G. 2000, J. Geophys. Res., 105, 2375

Lin, J. 2002, Chinese J. Astron. Astrophys., 2, 539

Lin, J. 2004, Sol. Phys., 222, 115

Lin, J., Ko, Y.-K., Sui, L., Raymond, J. C., Stenborg, G. A., Jiang, Y., Zhao, S., & Mancuso, S. 2005, ApJ, 622, 1251

Liu, W., Jiang, Y., Liu, S., & Petrosian, V. 2004, ApJ, 611, L53

Masuda, S., Kosugi, T., Hara, H., Tsuneta, S., & Ogawara, Y. 1994, Nature, 371, 495

Masuda, S., Kosugi, T., Hara, H., Sakao, T., Shibata, K., & Tsuneta, S. 1995, Publ. Astron. Soc. Japan, 47, 677

McKenzie, D.E. 2002, in Multi-Wavelength Observations of Coronal Structure and Dynamics, ed. Martens, P.C.H., Cauffman, D.P., 155

Melrose, D. B., & White, S. M. 1979, Proceedings of the Astronomical Society of Australia, 3, 369

Moore, R., McKenzie, D.L., Švestka, Z., Widing, K.G., & 12 co-authors 1980, in P.A. Sturrock (ed), Solar Flares, A Monograph from Skylab Solar Workshop II, p. 341

Petrosian, V., Donaghy, T. Q., & McTiernan, J. M. 2002, ApJ, 569, 459

Priest, E., & Forbes, T. 2002, Astron. Astrophys. Rev., 10, 313

Sakao, T., Kosugi, T., Masuda, S., Yaji, K., Inda-Koide, M., & Makishima, K. 1996, 17, pp(4/5)67

Shibata, K., Masuda, S., Shimojo, M., Hara, H., Yokoyama, T., Tsuneta, S., Kosugi, T., & Ogawara, Y. 1995, ApJ, 451, 83

Siarkowski M., & Falewicz, R. 2004, A&A, 428, 219

Smith, D. M., et al. 2002, Sol. Phys., 210, 33

Sturrock, P.A., 1966, Nature, 211, 695

Sui, L., Holman, G. D., Dennis, B. R., Krucker, S., Schwartz, R. A., & Tolbert, K. 2002,Sol. Phys., 210, 245

Sui, L., & Holman, G. D. 2003, ApJ, 596, L251

Sui, L., Holman, & G. D., Dennis, B. R. 2004, ApJ, 612, 546

Sui, L. 2005, Doctoral Dissertation, Catholic University of America

Sui, L., Holman, G. D., Dennis, B. R. 2005, ApJ, 626, 1102

Švestka, Z., Fontenla, J. M., Machado, M. E., Martin, S. T., Neidig, D. F. and Poletto, G. 1987, Sol. Phys., 169, 403

Tsuneta, S. 1996, ApJ, 456, 840

Tsuneta, S., Hara, H., Shimizu, T., Acton, L.W., Strong, K.T., Hudson, H.S., & Ogawara, Y. 1992, PASJ, 44, 63

Veronig, A. M., Brown, J. C. 2004, ApJ, 603, L117

Veronig, A. M., Karlickẙ, M., Vršnak, B., Temmer, M., Magdalenić, Dennis, B. R., Otruba, W., & Pötzi, W. 2005, A&A, submitted

Vourlidas, A., Subramanian P., Dere, K. P., & Howard, R. A. 2000, ApJ, 534, 456

Webb, D. F., Burkepile, J., Forbes, T. G., & Riley P. 2003, J. Geophys. Res., V108, Issue A12, pp. SSH 6-1

White, S. M., Krucker, S., Shibasaki, K., Yokoyama, T., Shimojo, M., & Kundu, M. R. 2003, 595, L111

White, S. M., Thomas, R. J., Schwartz, R. A. 2005, Solar Phys., 227, 231

Young, P. R., Del Zanna, G., Landi, E., Dere, K. P., Mason, H. E., Landini, M. 2003, Astro. J. Suppl. Series, 144, 135

Young, P. R., Landi, E., & Thomas, R. J. 1998, Astron. Astrophys., 329, 291
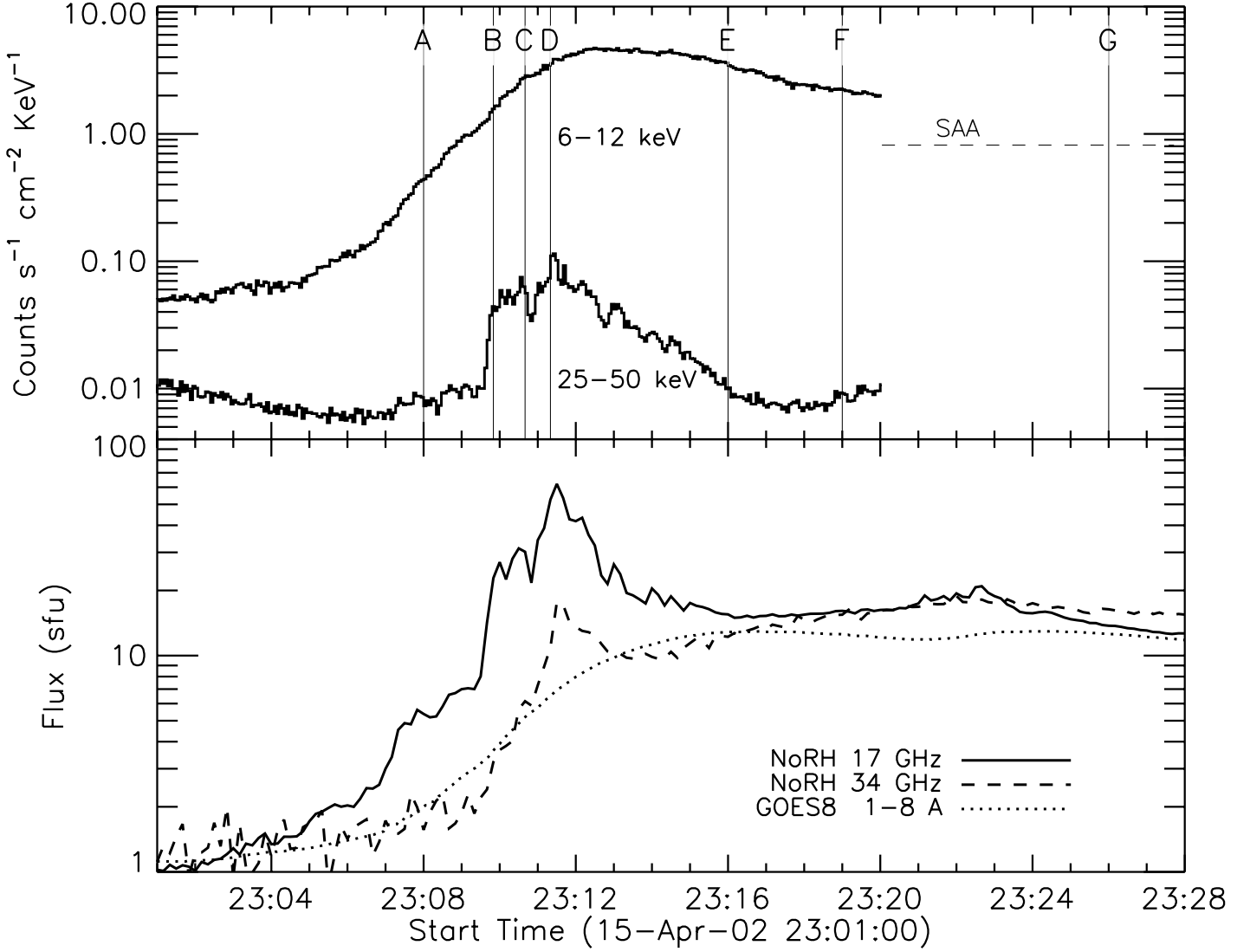
Fig. 1.— Light curves for the April 15 flare. The *upper panel* shows the RHESSI light curves in two energy bands. The *lower panel* shows the time profiles of the NoRH fluxes at 17 and 34 GHz. The GOES 1-8 Å flux is shown in the same plot with arbitrary units. The vertical lines labeled A-G indicate the start times of the images in Figs. 9 and 11.
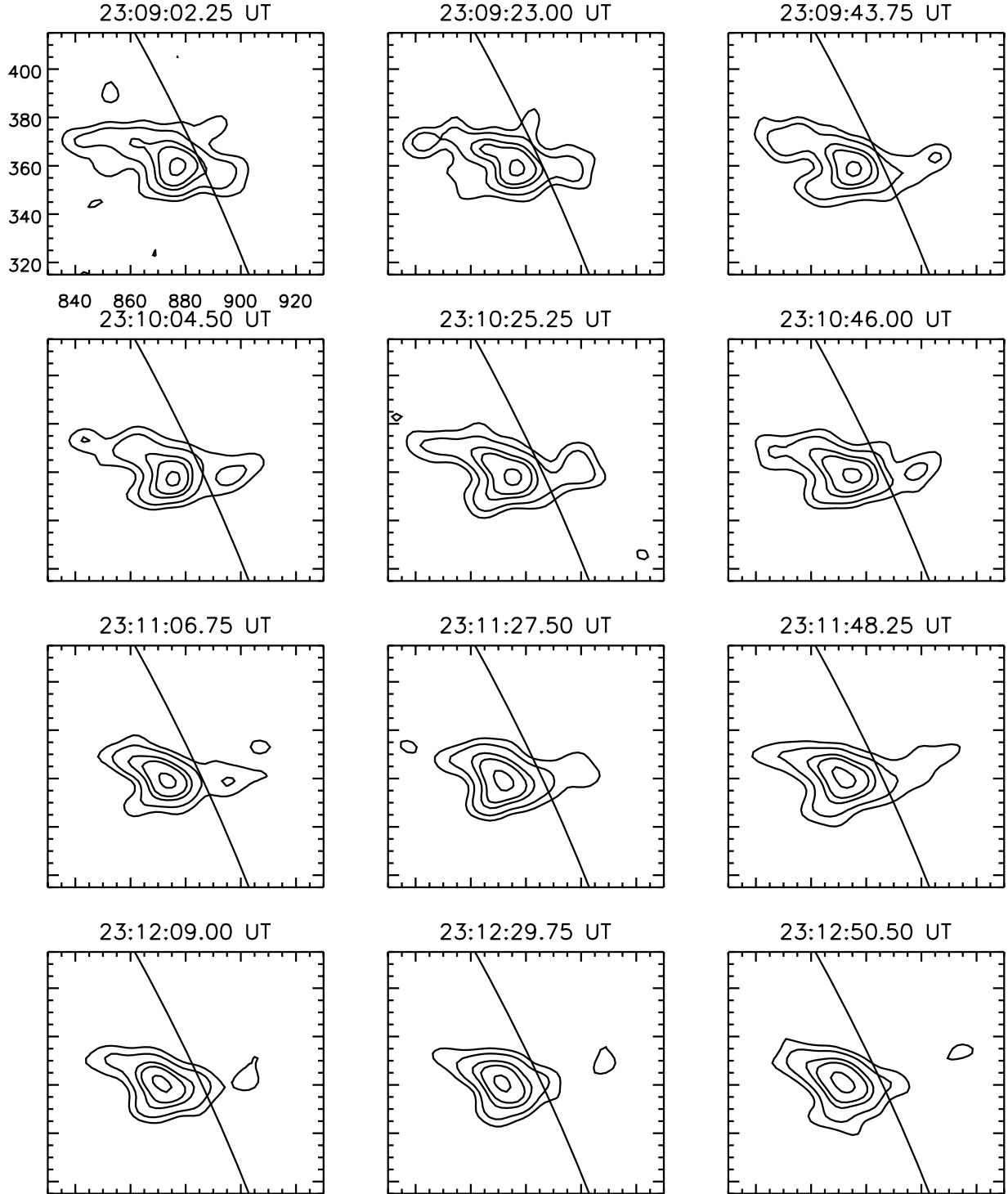
Fig. 2.— A time sequence of RHESSI 10–20 keV images for the 2002 April 15 flare. The images were reconstructed with the CLEAN algorithm using grids 3–9 and uniform weighting, giving an angular resolution of ∼ 7″. The accumulation time was 20 s. The start time of each 20 s image is indicated. The contour levels are 15, 25, 45, 60, and 90% of the peak flux in each image. The solid diagonal curve denotes the solar limb.
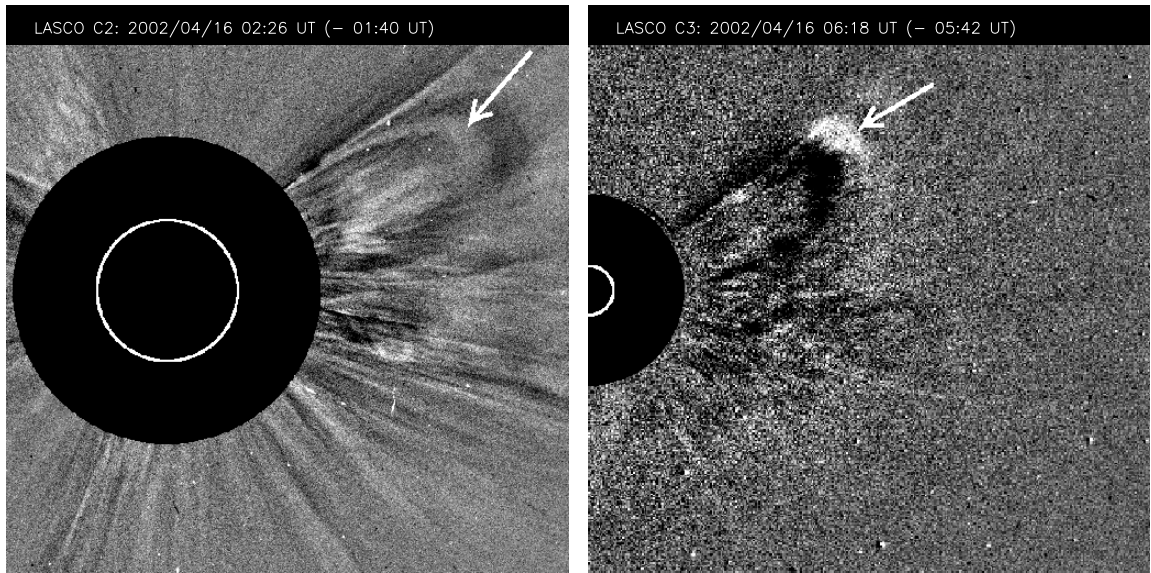
Fig. 3.— SOHO/LASCO C2 (left panel) and C3 (right panel) difference images on April 16, 2002. The arrow indicates the leading edge of the CME.
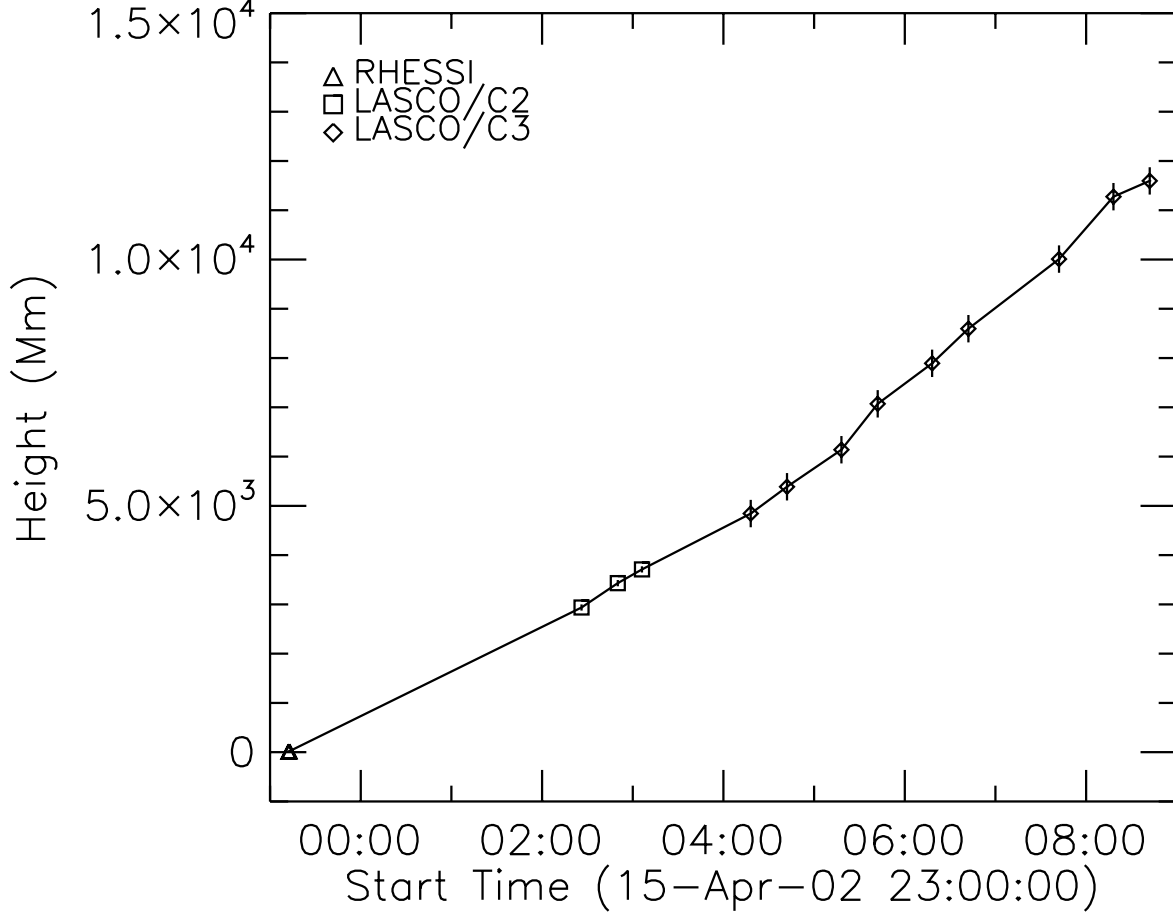
Fig. 4.— Height-time plot of the coronal source seen with RHESSI and the CME seen with LASCO C2/C3. The height is the altitude above the solar limb. The height of the coronal source is obtained with the three 10–20 keV images shown in the bottom row of Fig. 2. Because the time gap between those images (∼20 s) is short, the three data points appear like one in the plot. The uncertainty in the coronal source height is estimated to be 0.5 arcsec (∼0.4 Mm). Considering the faint nature of this CME, we take the measurement error for its leading edge to be 16 pixels, which is equivalent to a full error bar of 0.19 R$_\odot$ (∼132 Mm) for C2 and 0.94 R$_\odot$ (∼654 Mm) for C3.
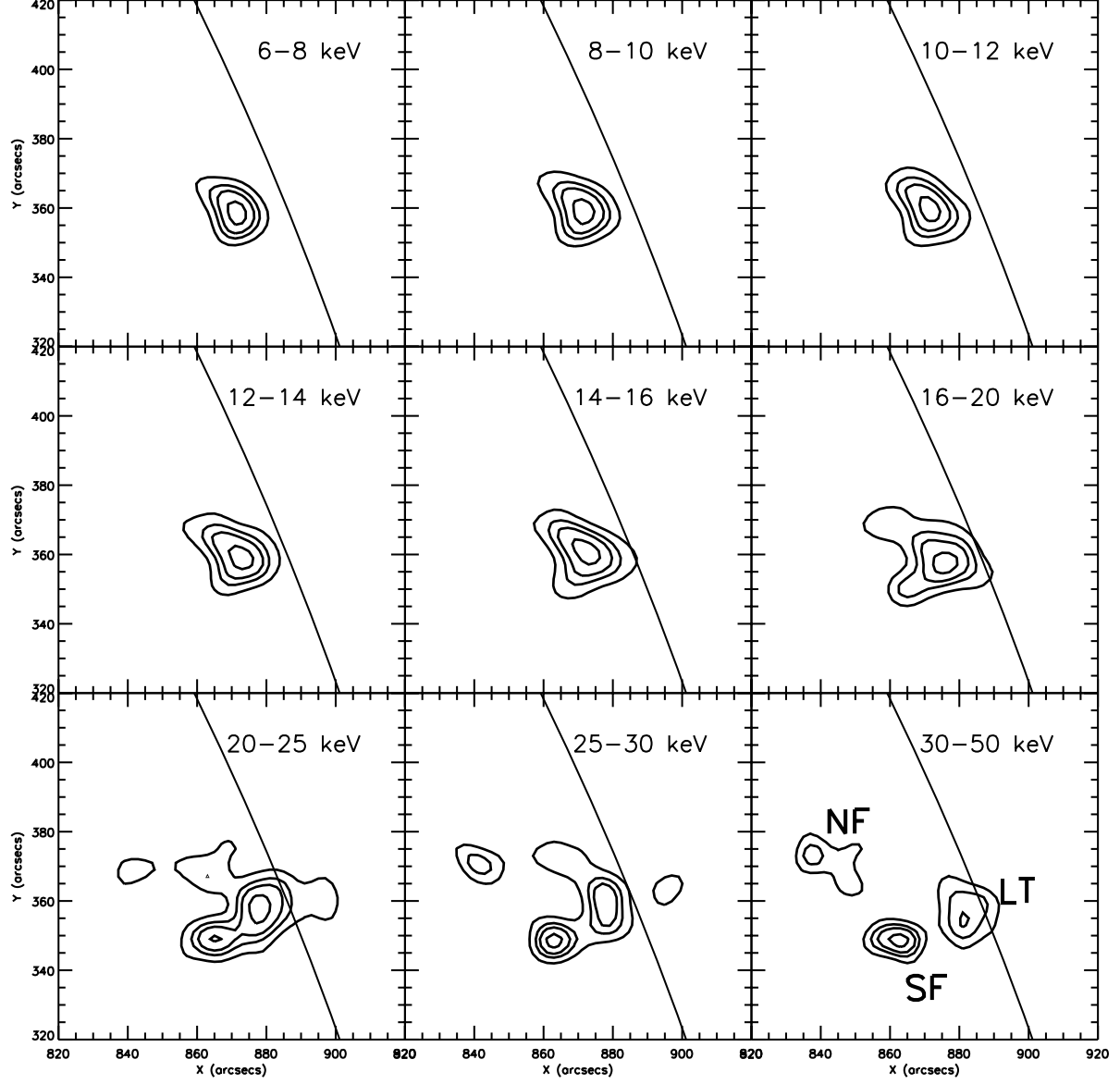
Fig. 5.— RHESSI images in different energy bands at the HXR peak (23:11–23:12 UT). The image reconstruction parameters are the same as in Fig. 2 except that the integration time is 1 min. The RHESSI contour levels are 35, 55, 70 and 90% of the peak flux in each image.
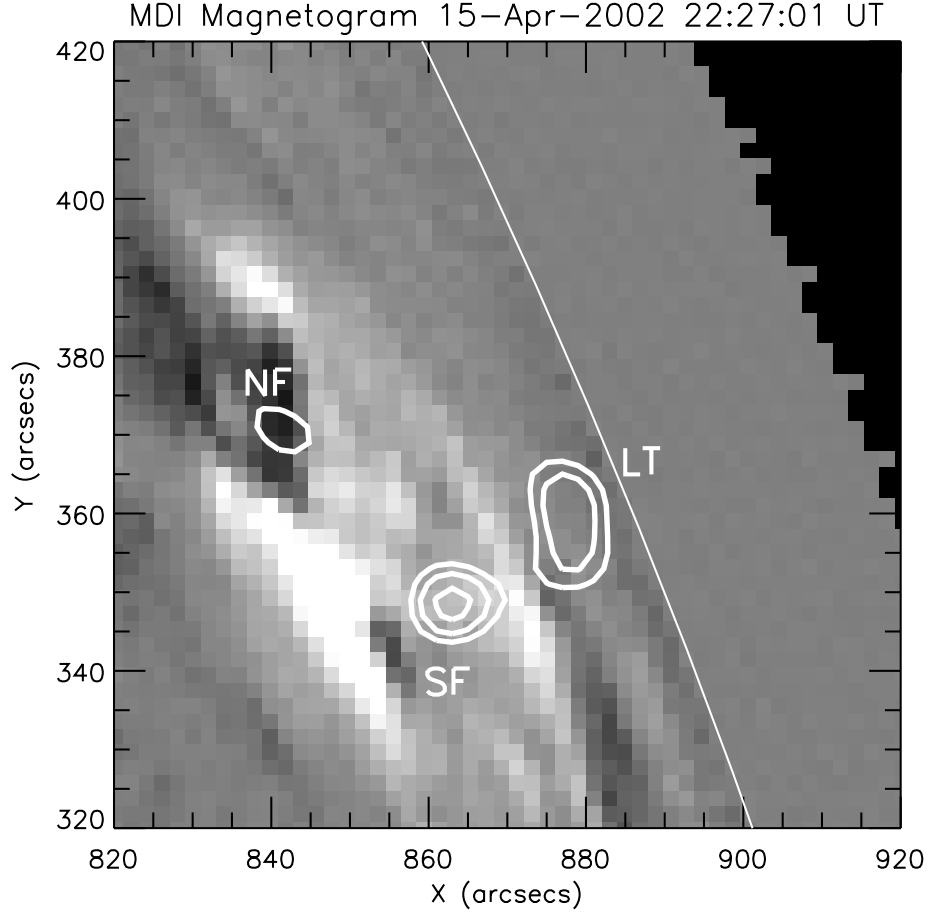
Fig. 6.— MDI magnetogram about 40 min before the flare started. The RHESSI 25–30 keV image at the major HXR peak is overlaid. The contour levels are 55, 70 and 90% of the peak flux. The maximal magnetic field strength at the northern ('NF') and southern ('SF') footpoints are -380 and +280 Gauss, respectively.
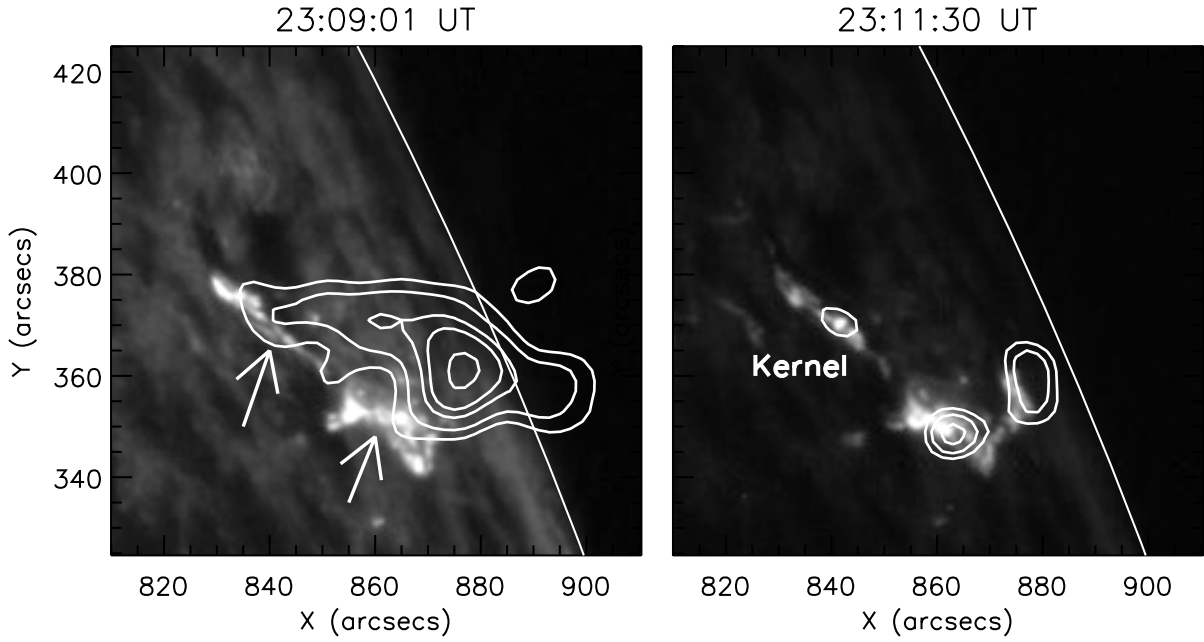
Fig. 7.— *Left Panel*: TRACE 1600 Å image at 23:09:01 UT (in the rise phase of the flare) overlaid with RHESSI 10–20 keV, 23:09:02.25 UT contours. The contour levels are 15, 25, 45, 60, and 90% of the peak flux. The arrows point to the two ribbons. *Right Panel*: TRACE 1600 Å image at 23:11:30 UT (at the HXR peak of the flare) overlaid with RHESSI 25–30 keV contours at the same time. The contour levels are the same as in Fig. 6.
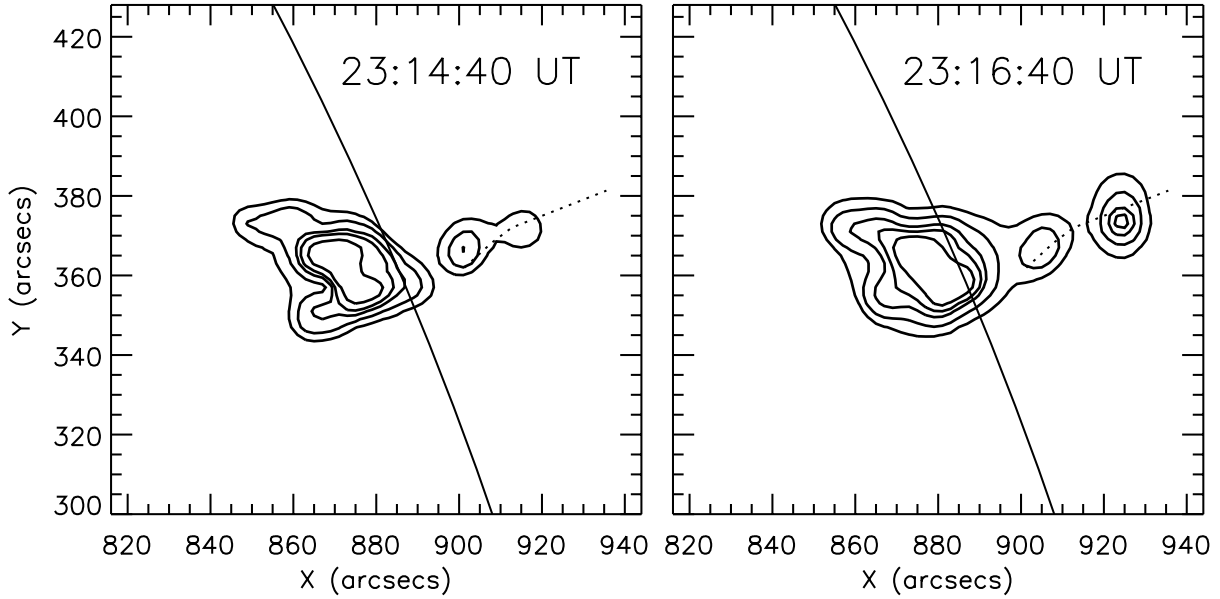
Fig. 8.— RHESSI 12–25 keV images at 23:14:40 UT (left panel) and 23:16:40 UT (right panel) showing coronal blobs believed to be evidence for magnetic islands produced by the tearing-mode instability along a current sheet above the flare loop. The images were constructed with the PIXON image algorithm (Hurford et al. 2002) using RHESSI grids 3–9. The integration time of each images is 20s. The contour levels are 5, 10, 20, 30, and 50% of the peak flux in each image. The dotted line indicates the trajectory taken by the coronal source above the loop shown in Fig. 2.
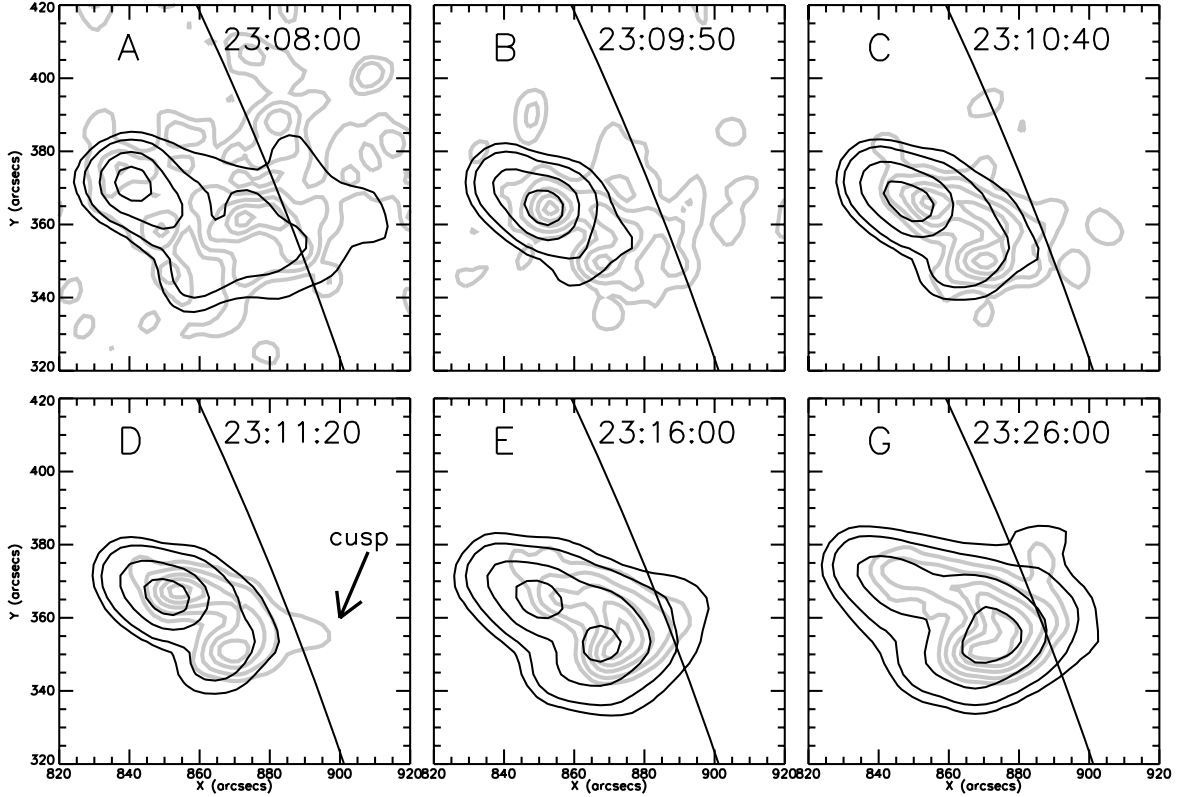
Fig. 9.— NoRH microwave images at 17 GHz (*dark contours*) and 34 GHz (*light contours*). The contour levels are 5, 10, 30, and 70% of the peak flux in each image for 17 GHz, and 17, 30, 50, 70, and 90% for the 34 GHz images. Based on the common features seen in both RHESSI and NoRH, the NoRH 17 and 34 GHz images were shifted by (+5, +4) and (-4, +5), respectively. The labels A-E and G correspond to the times marked on the lightcurves in Fig. 1.
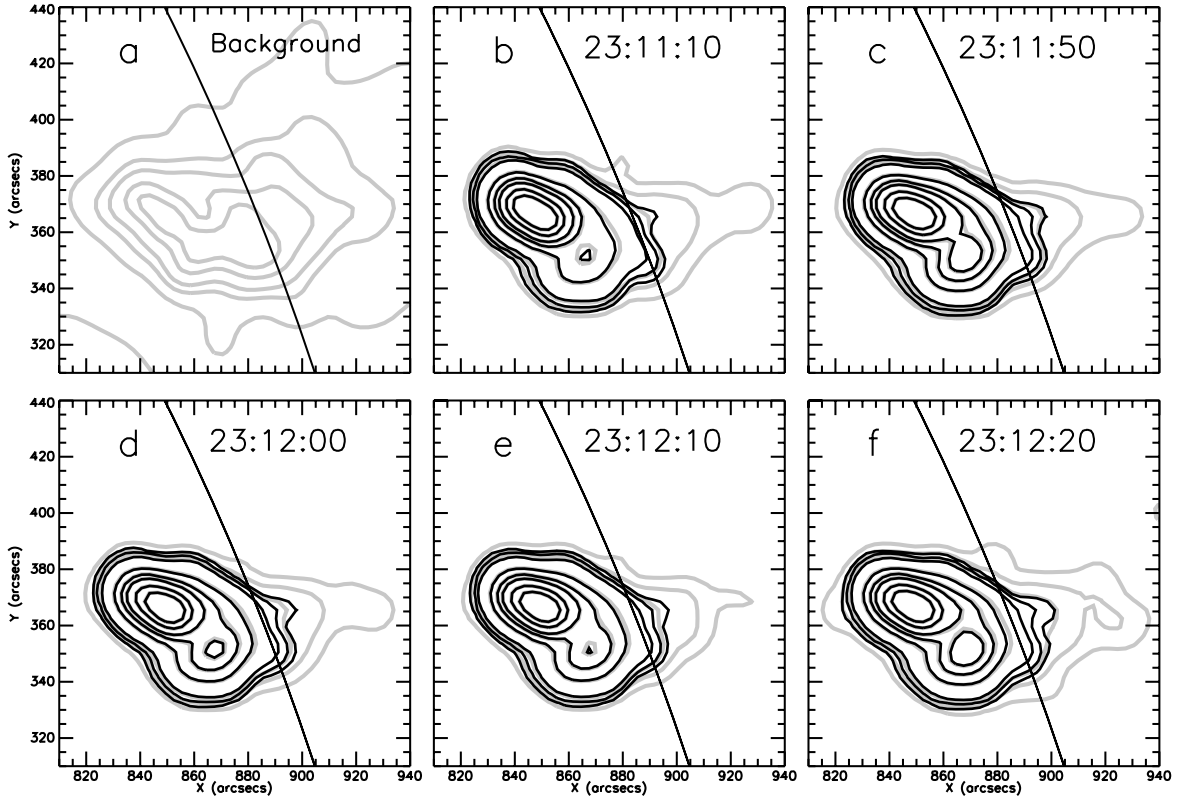
Fig. 10.— NoRH 17 GHz images before and after background subtraction during the impulsive phase of the flare. Panel 'a' shows the average of preflare 17 GHz images during the period 23:00–23:05 UT. In panel 'b' to 'f', the light and dark contours are the images before and after subtraction of the average of the preflare images. The contour levels are 0.5, 1, 2, 10, 20, 30, 50, and 70% of the peak flux in each image.
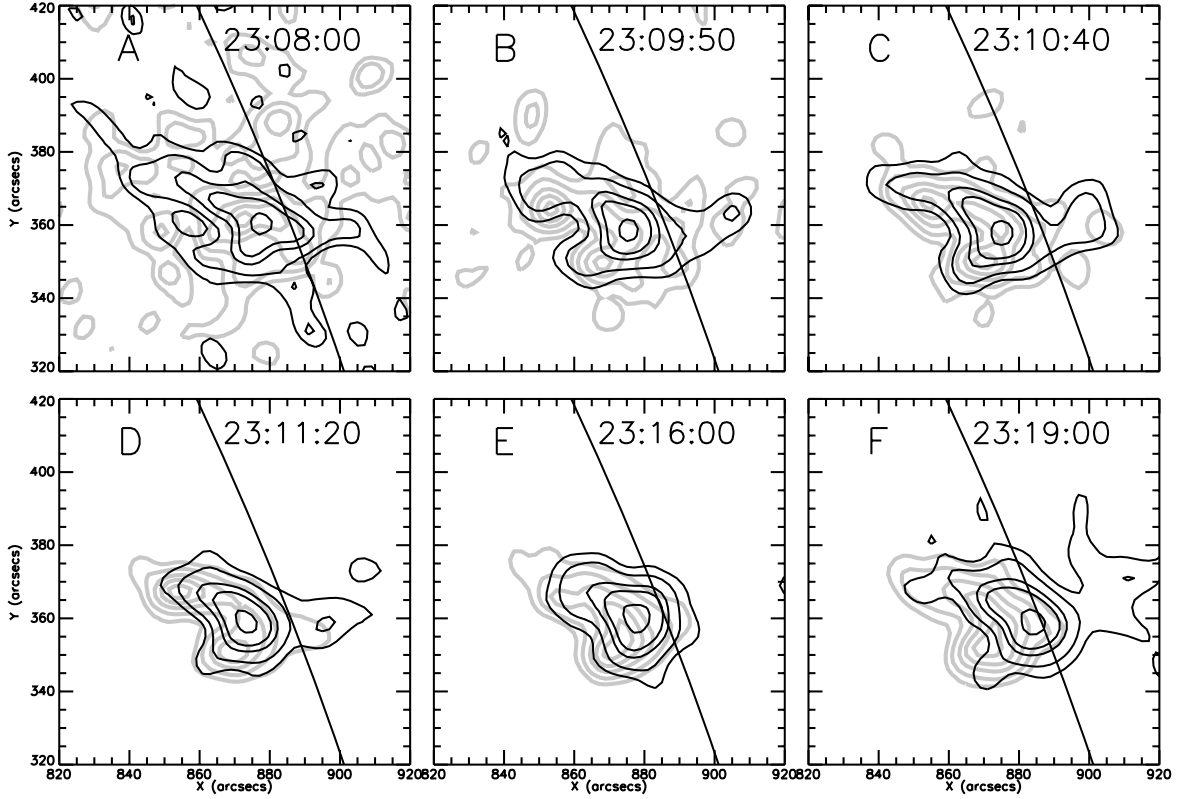
Fig. 11.— RHESSI 10–20 keV images (*dark contours*) and 34 GHz images (*light contours*). The contour levels are 15, 25, 45, 60, and 90% of the peak flux in each RHESSI image. The 34 GHz images are the same as in Fig. 9. The 34 GHz images were shifted the same amount as in Fig 9. The labels A–F correspond to the times marked on the lightcurve in Fig. 1.
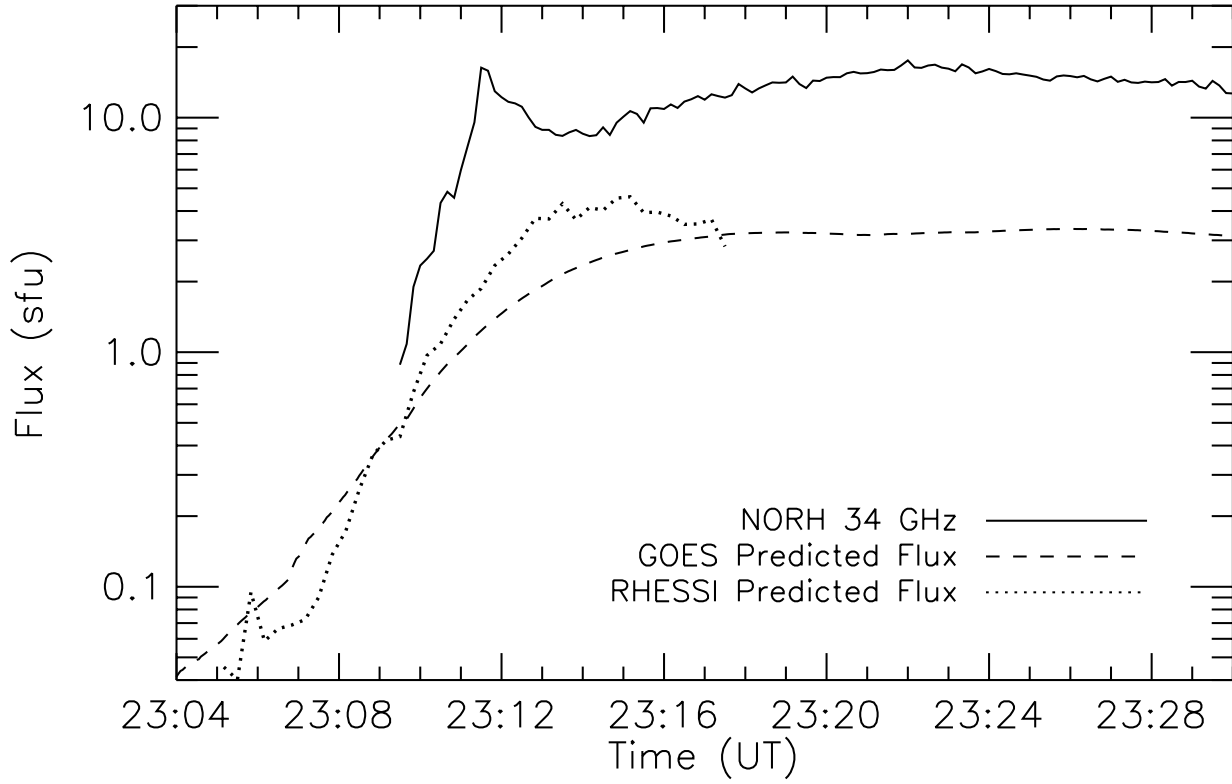
Fig. 12.— Comparison of NoRH 34 GHz fluxes and calculated microwave fluxes (assuming free-free emission) from the thermal plasma observed by GOES and RHESSI.